

Predicting tensile strength, hardness and corrosion rate of friction stir welded AA6061-T₆ aluminium alloy joints

S. Rajakumar^{*}, C. Muralidharan, V. Balasubramanian

Center for Materials Joining & Research (CEMAJOR), Department of Manufacturing Engineering, Annamalai University, Annamalai Nagar 608 002, Chidambaram, Tamil Nadu, India

ARTICLE INFO

Article history:

Received 17 September 2010

Accepted 9 December 2010

Available online 17 December 2010

Keywords:

A. Alloys

B. Welding

C. Hardness

ABSTRACT

AA6061-T₆ aluminium alloy (Al–Mg–Si alloy) has gathered wide acceptance in the fabrication of light weight structures requiring high strength-to-weight ratio and good corrosion resistance. The friction stir welding (FSW) process and tool parameters play major role in deciding the joint characteristics. In this research, the tensile strength and hardness along with the corrosion rate of friction-stir-butt welded joints of AA6061-T₆ aluminium alloy were investigated. The relationships between the FSW parameters (rotational speed, welding speed, axial force, shoulder diameter, pin diameter and tool hardness) and the responses (tensile strength, hardness and corrosion rate) were established. The optimal welding conditions to maximize the tensile strength and minimize the corrosion rate were identified and reported here.

© 2010 Elsevier Ltd. All rights reserved.

1. Introduction

The heat treatable wrought aluminium–magnesium–silicon alloys conforming to AA6061-T₆ have moderate strength and possess excellent welding characteristics compared to high strength aluminium alloys [1]. Hence, alloys of this class are extensively employed in marine frames, pipelines, storage tanks and aircraft applications. Although Al–Mg–Si alloys are readily weldable, they suffer from severe softening in the heat-affected zone (HAZ) because of reversion (dissolution) of Mg₂Si precipitates during the weld thermal cycle [2]. This type of mechanical impairment presents a major problem in engineering design [3]. Compared to many of the fusion welding processes that are routinely used for joining structural alloys, friction stir welding (FSW) is an emerging solid state joining process in which the material that is being welded does not melt and recast [4]. Defect-free welds with good mechanical properties have been made in a variety of aluminium alloys, even those previously thought to be non weldable [5]. When alloys are friction stir welded, phase transformations that occur during the cooling cycle of the weld are of a solid state type. Due to the absence of parent metal melting, the FSW process is observed to offer several advantages over fusion welding processes [6].

It is well known that whatever the welding method, the main challenge for the manufacturer is selecting the welding parameters

that would produce an excellent welded joint. Conventionally, to define the weld input parameters for new welded products to produce a welded joint with the required specifications is a time consuming trial accompanied by error development effort, with the weld input parameters chosen by the skill of the engineer or machine operator. Then the weld is inspected to determine whether it meets the specification or not. Eventually the chosen parameters would produce a welded joint close to the required specification. Also, what often not considered, or achieved are optimized welding parameter combinations. In other words, there are often alternative ideal welding parameters combinations that can be used if they can only be determined. To predict the welding parameters accurately without consuming time, materials and labour effort, various methods are available and one such method is response surface methodology (RSM).

Jayaraman et al. [7] developed an empirical relationship to predict tensile strength of friction stir welded of cast aluminium alloy using RSM. Elangovan and Balasubramanian [8] developed an empirical relationship to predict tensile strength of tensile properties of friction stir welded joints of AA2219 alloy using RSM. Lombord et al. [9] proposed a systematic approach to optimize FSW process parameters (tool rotational speed and feed rate) through consideration of frictional power input. Rajakumar et al. [10] developed mathematical models using RSM to analyze the effect of FSW process parameters and tool parameters on the tensile strength of AA7075 aluminium alloy. Lakshminarayanan and Balasubramanian [11] also studied the effect of FSW welding parameters on the tensile strength of butt joints made of AA7039 aluminium alloys using Taguchi parametric design approach.

It is important to investigate the mechanical properties of welded joint in order to describe its performance and the tensile

^{*} Corresponding author. Tel.: +91 09486870051 (mobile), +91 4144 231053 (R); fax: +91 4144 238080/238275.

E-mail addresses: srkcmajor@yahoo.com (S. Rajakumar), muralre@yahoo.co.in (C. Muralidharan), balasubramanian.v.2784@annamalaiuniversity.ac.in (V. Balasubramanian).

strength and hardness are the most vital mechanical properties. In this investigation, along with the tensile strength and hardness, the corrosion (resistance) rate was considered to evaluate the performance of the FSW joints of AA6061 alloy. Therefore in this paper, the first aim is to employ RSM to develop empirical relationships relating the FSW input parameters (rotational speed, welding speed, axial force, shoulder diameter, pin diameter and tool hardness) and the three output responses (i.e. tensile strength, hardness and corrosion rate). The second aim is to find the optimal welding combination that would maximize both the tensile strength and hardness and minimize the corrosion rate.

2. Methodology

2.1. Response surface methodology

Engineers often wish to determine the values of the input process parameters at which the responses reach their optimum. The optimum could be either a minimum or a maximum of a particular function in terms of the input parameters. Response surface methodology (RSM) is a collection of mathematical and statistical technique useful for analyzing problems in which several independent variables influence a dependent variable or response and the goal is to optimize the response [12]. In many experimental conditions, it is possible to represent independent factor in quantitative form as given in Eq. (1). Then these factors can be thought of as having a functional relationship or response as follows:

$$Y = \Phi(x_1, x_2, \dots, x_k) \pm e_r \quad (1)$$

Between the response Y and x_1, x_2, \dots, x_k of k quantitative factors, the function Φ is called response surface or response function. The residual e_r measures the experimental errors. For a given set of independent variables, a characteristic surface is responded. When the mathematical form of Φ is not known, it can be approximate satisfactorily within the experimental region by polynomial. In the present investigation, RSM was applied for developing the mathematical model in the form of multiple regression equations for the quantitative characteristics of the friction stir welded AA6061-T₆ aluminium alloy. In applying the RSM, the independent variable was viewed as a surface to which a mathematical model is fitted. Representing the tensile strength of the joint by TS, the response is a function of tool rotational speed (N), welding speed (S), axial force (F), shoulder diameter (D), pin diameter (P) and tool hardness (H) and it can be expressed as:

$$Y = f(N, S, F, D, P, H)$$

The second order polynomial (regression) equation used to represent the response surface 'Y' is given by [13]:

$$Y = b_0 + \sum b_i x_i + \sum b_{ii} x_i^2 + \sum b_{ij} x_i x_j + e_r \quad (2)$$

Due to wide ranges of parameters, it was decided to use six factors, five levels, central composite design matrix to optimize the experimental conditions. Table 3 shows the 52 set of coded conditions used to form the design matrix. First 32 experimental conditions are derived from full-factorial experimental design matrix ($2^5 = 32$). All the variables at the intermediate (0) level constitute the centre points while the combinations of each process variable either at its lowest (−2.378) or its highest (+2.378) with the other twelve variables of the intermediate levels constitute the star points. Thus the 52 experimental conditions allowed the estimation of the linear, quadratic and two-way interactive effects of the variables on the tensile strength of welded joints. The method of designing such a matrix is dealt with elsewhere [14,15]. For the convenience of recording and processing experimental data, upper

and lower levels of the factors were coded as +2.378 and −2.378 respectively. The coded values of any intermediate value can be calculated, using the following relationship:

$$X_i = 2[2X - (X_{\max} + X_{\min})]/(X_{\max} - X_{\min}) \quad (3)$$

where X_i is the required coded value of a variable X ; X is any value of the variable from X_{\min} to X_{\max} ; X_{\min} is the lower level of the variable; X_{\max} is the highest level of the variable.

2.2. Experimental design

The test was designed based on a six factors, five levels central composite rotatable design with half replication [12]. The friction stir-welding input variables are rotational speed, welding speed, axial force, shoulder diameter, pin diameter and tool hardness. In order to find the range of each input parameters, trial experiments were performed by changing one parameter at a time while keeping other process parameters at a constant setting. Absence of macro level welding defects, smooth and uniform welded surface with the sound face were the criteria for selecting the feasible working range. Table 1 displays the macrographs to provide the evidence for fixing the feasible working range of welding parameters. Table 2 shows the process variables, their coded and actual values. Statistical software Design-Expert V8 was used to code the variables and to establish the design matrix (shown in Table 3). RSM was applied to the experimental data using the same software, polynomial Eq. (2) was fitted to the experimental data to obtain the regression equations for all responses. The statistical significance of the terms in each regression equation was examined using the sequential F -test, lack-of-fit test and other adequacy measures using the same software to obtain the best fit.

2.3. Desirability approach

There are many statistical techniques for solving multiple response problems like overlaying the contours plot for each response, constrained optimization problems and desirability approach. The desirability method is recommended due to its simplicity, availability in the software and provides flexibility in weighing and giving importance for individual response. Solving such multiple-response optimization problems using this technique involves for combining multiple responses into a dimensionless measure of performance called the overall desirability function. The desirability approach involves transforming each estimated response, Y_i , into a unitless utility bounded by $0 < d_i < 1$, where a higher d_i value indicates that response value Y_i is more desirable, if $d_i = 0$ this means a completely undesired response [16].

In the current work, the individual desirability of each response, d_i , was calculated using Eqs. (4)–(7). The shape of the desirability function can be changed for each goal by the weight field 'wt'. Weights are used to give more emphasis to the upper/lower bounds or to emphasize the target value. Weights could be ranged between 0.1 and 10; a weight greater than 1 gives more emphasis to the goal, while weights less than 1 give less emphasis. When the weight value is equal to 1, this will make the d_i s vary from 0 to 1 in a linear mode. In the desirability objective function (D), each response can be assigned an importance (r), relative to the other responses. Importance varies from the least important value of 1, indicated by (+), the most important value of 5, indicated by (++++). If the varying degrees of importance are assigned to the different responses, the overall objective function is shown in Eq. (7) below. Where n is the number of responses in the measure and T_i is the target value of i th response [17].

Table 1
Macrostructure observation of AA6061-T₆ aluminium alloy.





Input parameters	Parameter range	Macrostructure	Name of the defect	Probable reason
Rotational speed	<800 rpm		Tunnel defect	In sufficient heat generation and insufficient metal transportation
Rotational speed	>1400 rpm		Pin hole	Further increase in turbulence of the plasticized metal
Welding speed	<30 mm/min		Tunnel defect	Excess heat input per unit length of the weld and no vertical movement of the metal
Welding speed	>130 mm/min		Kissing defect	Increase in welding speed resulted in poor plasticization of metal and associated defect
Axial force	<5 kN		Tunnel hole	In sufficient axial force and in adequate heat generation
Axial force	>11 kN		Worm hole	Additional axial force leads to excess heat input and thinning of the weld zone
Shoulder diameter	<7 mm		Pin hole	Insufficient stirring butt surfaces could be directly bonded without the metallic bond between oxide free surfaces in the root part of the weld
Shoulder diameter	>22.5 mm		Pin hole	Excessive heat input due to softening and work hardening effect
Pin diameter	<2.5 mm		Piping defect	Asymptote heat generation and Insufficient metal transportation
Pin diameter	>7.5 mm		Tunnel defect	Excessive heat input due to softening
Tool hardness	<33 HRC		Pin hole	Due to low frictional heat generation
Tool Hardness	>56 HRC		Worm hole	High frictional heat generation

Table 2Important FSW process parameters and their levels for AA6061-T₆ aluminium alloy.

#	Parameter	Notation	Unit	Levels				
				(−2.378)	(−1)	(0)	(+1)	(+2.378)
1	Rotational speed	<i>N</i>	rpm	862	1000	1100	1200	1337
2	Welding speed	<i>S</i>	mm/min	32.43	60	80	100	127.5
3	Axial force	<i>F</i>	kN	5.62	6	7	8	10.37
4	Shoulder diameter	<i>D</i>	mm	7.86	12	15	18	22.13
5	Pin diameter	<i>P</i>	mm	2.6	4	5	6	7.37
6	Tool hardness	<i>H</i>	HRC	33	40	45	50	56

Table 3

Design matrix.

Experimental details							Results		
Exp. No.	Input parameters						Responses		
	<i>N</i>	<i>S</i>	<i>F</i>	<i>D</i>	<i>P</i>	<i>H</i>	TS (MPa)	<i>H</i> (HV)	CR (mm/y) × 10 ^{−4}
1	−1	−1	−1	−1	−1	−1	165	64	6.49
2	1	−1	−1	−1	−1	1	179	71	4.3
3	−1	1	−1	−1	−1	1	182	68	4.93
4	1	1	−1	−1	−1	−1	178	75	4.08
5	−1	−1	1	−1	−1	1	191	70	6.13
6	1	−1	1	−1	−1	−1	195	79	5.33
7	−1	1	1	−1	−1	−1	191	67	5.44
8	1	1	1	−1	−1	1	202	84	3.9
9	−1	−1	−1	1	−1	1	184	68	5.69
10	1	−1	−1	1	−1	−1	190	79	3.47
11	−1	1	−1	1	−1	−1	180	69	4.62
12	1	1	−1	1	−1	1	195	86	3.4
13	−1	−1	1	1	−1	−1	185	69	5.58
14	1	−1	1	1	−1	1	192	87	4.4
15	−1	1	1	1	−1	1	191	76	5.34
16	1	1	1	1	−1	−1	202	88	4.16
17	−1	−1	−1	−1	1	1	182	70	5.96
18	1	−1	−1	−1	1	−1	188	84	5.02
19	−1	1	−1	−1	1	−1	178	70	6.5
20	1	1	−1	−1	1	1	193	89	4.14
21	−1	−1	1	−1	1	−1	184	69	6.43
22	1	−1	1	−1	1	1	191	91	4.19
23	−1	1	1	−1	1	1	194	76	5.39
24	1	1	1	−1	1	−1	202	89	4.4
25	−1	−1	−1	1	1	−1	191	70	4.23
26	1	−1	−1	1	1	1	202	91	2.22
27	−1	1	−1	1	1	1	198	75	4.5
28	1	1	−1	1	1	−1	206	93	3.22
29	−1	−1	1	1	1	1	172	75	4.37
30	1	−1	1	1	1	−1	200	94	3.02
31	−1	1	1	1	1	−1	188	72	4.79
32	1	1	1	1	1	1	200	102	3.42
33	−2.378	0	0	0	0	0	187	58	6.49
34	2.378	0	0	0	0	0	207	95	5.51
35	0	−2.378	0	0	0	0	186	75	3.39
36	0	2.378	0	0	0	0	196	83	5.01
37	0	0	−2.378	0	0	0	188	76	4.4
38	0	0	2.378	0	0	0	201	86	4.15
39	0	0	0	−2.378	0	0	184	75	4.89
40	0	0	0	2.378	0	0	198	88	5.47
41	0	0	0	0	−2.378	0	188	79	2.93
42	0	0	0	0	2.378	0	198	96	3.93
43	0	0	0	0	0	−2.378	186	74	3.22
44	0	0	0	0	0	2.378	191	82	4.78
45	0	0	0	0	0	0	222	120	3.89
46	0	0	0	0	0	0	226	121	1.13
47	0	0	0	0	0	0	225	122	1.14
48	0	0	0	0	0	0	221	119	1.16
49	0	0	0	0	0	0	220	121	0.83
50	0	0	0	0	0	0	223	121	0.87
51	0	0	0	0	0	0	226	122	0.77
52	0	0	0	0	0	0	222	123	1.11

TS – tensile strength; H – hardness; CR – corrosion rate.

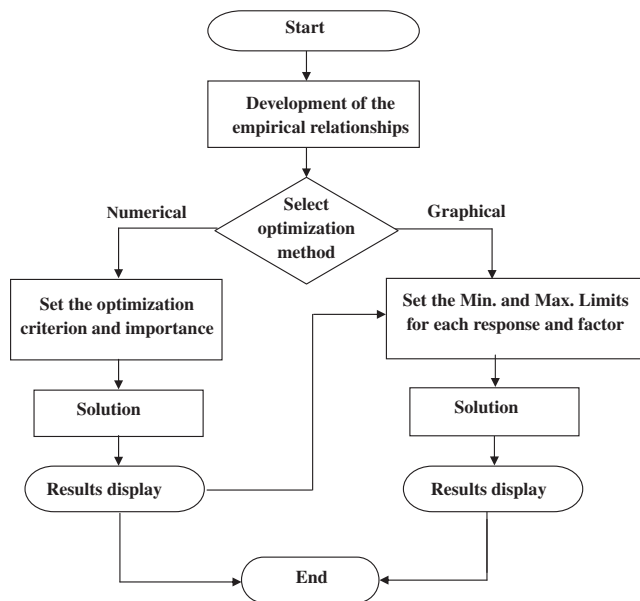


Fig. 1. Flow chart for optimization steps.

For goal of maximum, the desirability will be defined by

$$d_i = \begin{cases} 0, & Y_i \leq \text{Low}_i \\ \left(\frac{Y_i - \text{Low}_i}{\text{High}_i - \text{Low}_i} \right)^{wt_i}, & \text{Low}_i < Y_i < \text{High}_i \\ 1, & Y_i \geq \text{High}_i \end{cases} \quad (4)$$

For goal of minimum, the desirability will be defined by:

$$d_i = \begin{cases} 1, & Y_i \leq \text{Low}_i \\ \left(\frac{\text{High}_i - Y_i}{\text{High}_i - \text{Low}_i} \right)^{wt_i}, & \text{Low}_i < Y_i < \text{High}_i \\ 0, & Y_i \geq \text{High}_i \end{cases} \quad (5)$$

For goal as a target, the desirability will be defined by:

$$d_i = \begin{cases} \left(\frac{Y_i - \text{Low}_i}{T_i - \text{Low}_i} \right)^{wt_{1i}}, & \text{Low}_i < Y_i < T_i \\ \left(\frac{Y_i - \text{High}_i}{T_i - \text{High}_i} \right)^{wt_{2i}}, & T_i < Y_i < \text{High}_i \\ 0, & \text{Otherwise} \end{cases} \quad (6)$$

For goal within range, the desirability will be defined by:

$$d_i = \begin{cases} 1, & \text{Low}_i < Y_i < \text{High}_i \\ 0, & \text{Otherwise} \end{cases} \quad (7)$$

$$D = \left(\prod_{i=1}^n d_i^{r_i} \right)^{1/\sum r_i}$$

2.4. Optimization

The optimization part in Design-Expert software V8 searches for a combination of factor levels that simultaneously satisfy the requirements placed (i.e. optimization criteria) on each one of the responses and process factors (i.e. multiple-response optimization). Numerical and graphical optimization methods were used in this

work by selecting the desired goals for each factor and response. As mentioned before, the numerical optimization process involves combining the goals into an overall desirability function (D). The numerical optimization feature in the design-expert package finds one point or more in the factors domain that would maximize this objective function. In a graphical optimization with multiple responses, the software defines regions where requirement simultaneously meet the proposed criteria. Also, superimposing or overlaying critical response contours can be defined on a contour plot. Then, a visual search for the best compromise becomes possible. In case of dealing with the many responses, it is recommended to run numerical optimization first; otherwise it is impossible to find out a feasible region. The graphical optimization displays the area of feasible response values in the factor space. Regions that do not fit the optimization criteria are shaded [17]. Fig. 1 shows flow chart of the optimization steps in the Design-Expert software.

3. Experimental work

The rolled plates of 5 mm thickness, medium strength AA6061-T₆ aluminium alloy was used as base metal. Chemical composition and mechanical properties of the base metal are shown in Table 4. The plate was cut to the required size (300 mm × 150 mm) by power hacksaw followed by milling. The square butt joint configuration (300 mm × 300 mm) was prepared to fabricate FSW joints. The initial joint configuration was obtained by securing the plates in position using mechanical clamps. The direction of welding was normal to the rolling direction. Single pass welding procedure was followed to fabricate the joints. Non-consumable tools made of high carbon steel were used to fabricate the joints. Based on six factors, five level central composite designs, 15 tools were made with different tool pin diameter, shoulder diameter and tool hardness. Five levels of tool hardness were obtained by heat treating high carbon steel in different quenching media (air, oil, water, furnace cooling). An indigenously designed and developed computer numerical controlled friction stir welding machine (22 kW; 4000 rpm; 60 kN) was used to fabricate the joints. As prescribed by the design matrix, 52 joints were fabricated. The tensile specimens comprising the welded joints were machined to the required dimensions (Fig. 2) as per ASTM E8M-04 guidelines [18]. The tensile test was carried out in 100 kN, servo controlled universal testing machine (Make: FIE – BLUESTAR, INDIA, Model: UNITEK 94100) with a cross head speed of 0.5 mm/min at room temperature. From each joint, three tensile specimens were prepared and the average of three results is presented in Table 2. The images of the specimens before and after the tensile test are shown in Fig. 3. Vickers's micro hardness testing machine (Make: Shimadzu and Model: HMV-2T) was employed for measuring the hardness of the weld nugget region with 0.05 kg load at 15 s. The friction stir welded specimens were cut to the dimensions of 10 mm × 10 mm × 5 mm

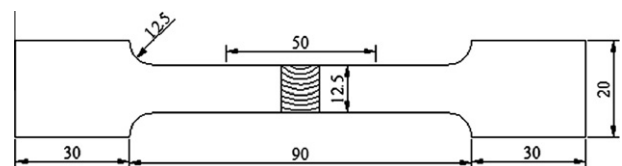


Fig. 2. Dimensions of flat tensile specimens (in mm).

Table 4
Chemical composition (wt.%) and mechanical properties of base metal.

Chemical composition							Mechanical properties			
Alloy	Si	Fe	Cu	Mn	Mg	Al	Yield strength (MPa)	Ultimate tensile strength (MPa)	Elongation (%)	Hardness (0.05 kg at 15 s) (HV)
AA6061-T ₆	0.58	0.35	0.22	0.12	1.1	Bal	235	283	26	105

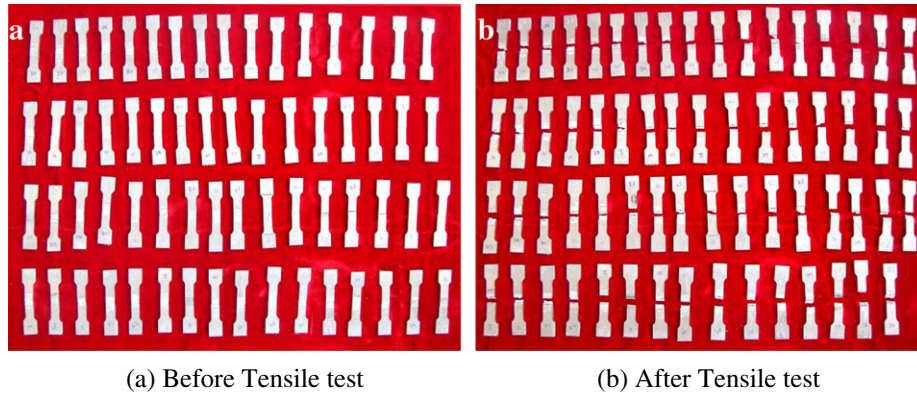


Fig. 3. Tensile specimens.

to evaluate the corrosion rate by immersion test method. Fig. 4 presents corrosion test samples. The specimens were ground with 500#, 800#, 1200#, 1500# grit SiC paper washed with distilled water and dried by warm flowing air. The corrosion rates of the AA6061-T₆ alloy were estimated through the weight loss measurement. The original weight (W_0) of the specimen were recorded and then immersed in the solution of 3.5% NaCl solution for 24 h. Finally, the corrosion products were removed by immersing the specimens for one minute in the solution prepared by using 50 g chromium trioxide (CrO_3), 2.5 g silver nitrate (AgNO_3) and 5 g barium nitrate ($\text{Ba}(\text{NO}_3)_2$) for 250 ml distilled water. The final weight (wt) of the specimen was measured and the net weight loss was calculated using the following equation [19]:

$$\text{Corrosion rate (CR)} = \frac{87.6 \times W}{A \times D \times T} \quad (8)$$

where W = weight loss in mg, A = surface area of the specimen in cm^2 , D = density of the material, 2.7 g/cm^3 , T = corrosion time in h.

4. Results and discussion

4.1. Development of empirical relationships

The fit summary tab in the Design-Expert software suggests the highest order of polynomial where the additional terms are significant and the model is not aliased. The tensile strength, hardness and corrosion rate of the weld nugget of FSW joints are function of rotational speed (N), welding speed (S), axial force (F), shoulder diameter (D), pin diameter (P) and tool hardness (H) and it can be expressed as:

$$\text{Tensile strength (TS)} = f(N, S, F, D, P, H) \quad (9)$$

$$\text{Weld nugget hardness (WH)} = f(N, S, F, D, P, H) \quad (10)$$

$$\text{Corrosion rate (CR)} = f(N, S, F, D, P, H) \quad (11)$$

and for six factors, the selected polynomial could be expressed as:

$$\begin{aligned} (\text{TS}) \text{ or } (\text{WH}) \text{ or } (\text{CR}) = & b_0 + b_1(N) + b_2(S) + b_3(F) + b_4(D) \\ & + b_5(P) + b_6(H) + b_{11}(N^2) + b_{22}(S^2) \\ & + b_{33}(F^2) + b_{44}(D^2) + b_{55}(P^2) + b_{66}(H^2) \\ & + b_{12}(NS) + b_{13}(NF) + b_{14}(ND) \\ & + b_{15}(NP) + b_{16}(NH) + b_{23}(SF) \\ & + b_{24}(SD) + b_{25}(SP) + b_{26}(SH) \\ & + b_{34}(FD) + b_{35}(FP) + b_{36}(FH) \\ & + b_{45}(DP) + b_{46}(DH) + b_{56}(PH) \end{aligned} \quad (12)$$

where b_0 is the average of responses and b_1, b_2, \dots, b_{66} are the coefficients that depend on respective main and interaction effects of

the parameters. The value of the coefficient was calculated using the following expressions:

$$b_0 = 0.110749 \left(\sum 0y \right) - 0.018738 \sum (X_{iij}) \quad (13)$$

$$b_i = 0.023087 \sum (X_{iy}) \quad (14)$$

$$\begin{aligned} b_{ii} = & 0.0152625 \sum (X_{iij}) + 0.001217 \sum \sum (X_{iij}) \\ & - 0.018738 \left(\sum y \right) \end{aligned} \quad (15)$$

$$b_{ij} = 0.03125 \sum (X_{iij}) / n \quad (16)$$

All the coefficients were tested for their significance at 95% confidence level applying Fisher's F -test using Design-Expert V8 statistical software package. After determining the significant coefficients, the final models were developed using only these coefficients and the final empirical relationships to estimate tensile strength, hardness and corrosion rate of weld nugget, developed by the above procedure are given below:

(i) Tensile strength:

$$\begin{aligned} (\text{TS}) = & \{223.18 + 4.77(N) + 2.60(S) + 2.77(F) \\ & + 2.64(D) + 2.10(P) + 0.85(H) + 1.16(ND) \\ & + 0.97(NP) - 1.22(NH) + 0.97(SF) + 1.09(SH) \\ & - 3.78(FD) - 3.22(FP) - 1.66(FH) - 1.28(DH) \\ & - 1.09(PH) - 4.74(N^2) - 5.80(S^2) - 5.19(F^2) \\ & - 5.80(D^2) - 5.45(P^2) - 6.25(H^2)\} \text{ MPa} \end{aligned} \quad (17)$$

(ii) Weld nugget hardness:

$$\begin{aligned} (\text{WH}) = & \{121.11 + 7.90(N) + 1.55(S) + 2.07(F) \\ & + 2.51(D) + 3.47(P) + 1.55(H) + 0.37(NS) \\ & + 0.81(NF) + 1.19(ND) + 1.81(NP) \\ & + 0.56(SH) - 0.44(FP) + 0.62(FH) \\ & - 7.85(N^2) - 7.40(S^2) - 7.05(F^2) - 6.96(D^2) \\ & - 5.90(P^2) - 7.58(H^2)\} \text{ HV} \end{aligned} \quad (18)$$

(iii) Corrosion rate:

$$\begin{aligned} (\text{CR}) = & \{1.76 - 0.68(N) - 0.09(S) + 0.06(F) - 0.46(D) \\ & - 0.12(P) - 0.09(H) + 0.09(NS) + 0.08(NF) \\ & + 0.17(SD) + 0.20(SP) + 0.15(FD) - 0.07(FP) \\ & - 0.29(DP) + 0.13(DH) - 0.10(PH) + 0.88(N^2) \\ & + 0.56(S^2) + 0.52(F^2) + 0.64(D^2) + 0.43(P^2) \\ & + 0.53(H^2)\} \text{ mm/y} \end{aligned} \quad (19)$$

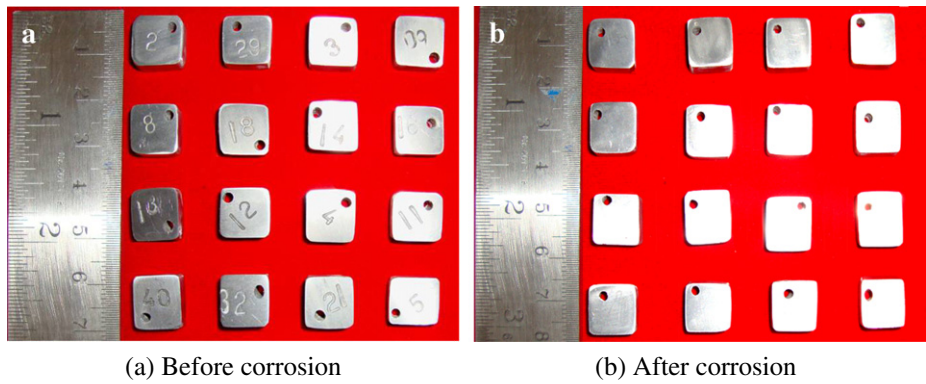


Fig. 4. corrosion specimens.

The adequacy of the developed empirical relationship was tested using the analysis of variance (ANOVA) technique [12]. Table 5 shows the ANOVA test results for the tensile strength, hardness and corrosion rate, respectively. As per this technique,

Table 5
ANOVA test results.

Terms	Tensile strength (TS)	Weld nugget hardness (WH)	Corrosion rate (CR)
<i>First-order terms</i>			
Sum of squares (SS)	2134.155	3890.338	3.08×10^{-7}
Degrees of freedom (d.f.)	6	6	6
Mean squares (MS)	355.6924	648.389	5.14×10^{-7}
<i>Second-order terms</i>			
Sum of squares (SS)	10671.98	16295.18	1.29×10^{-6}
Degrees of freedom (d.f.)	27	27	27
Mean squares (MS)	395.2586	603.5252	4.79×10^{-8}
<i>Error order terms</i>			
Sum of squares (SS)	36.875	10.875	2.31×10^{-9}
Degrees of freedom (d.f.)	7	7	7
Mean squares (MS)	5.267	1.553	3.30×10^{-10}
<i>Lack of fit</i>			
Sum of squares (SS)	64.14368	6.945318	5.20×10^{-8}
Degrees of freedom (d.f.)	17	17	17
Mean squares (MS)	3.773	0.408	3.05×10^{-9}
F-ratio	2.37	2.37	2.37
Prob > F	93.905	812.814	153.13
R ²	0.9906	0.9989	99.4%
R _{ratio} (calculated)	0.9542	0.9962	97.3%
R _{ratio} (from table) (33,7,0.05)	2.30	2.30	2.30
Model	Significant	Significant	Significant

SS – sum of squares, MS – mean squares, d.f. – degrees of freedom, F – Fisher’s ratio.

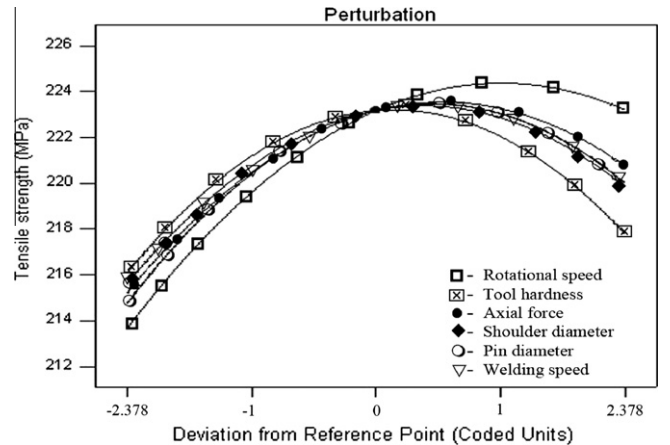


Fig. 5. Perturbation plot showing the effect of all factors on the tensile strength.

if the calculated value of the *F*-ratio of the developed model is less than the standard *F*-ratio (from *F*-table) value at a desired level of confidence (say 95%), then the model is said to be adequate within the confidence limit.

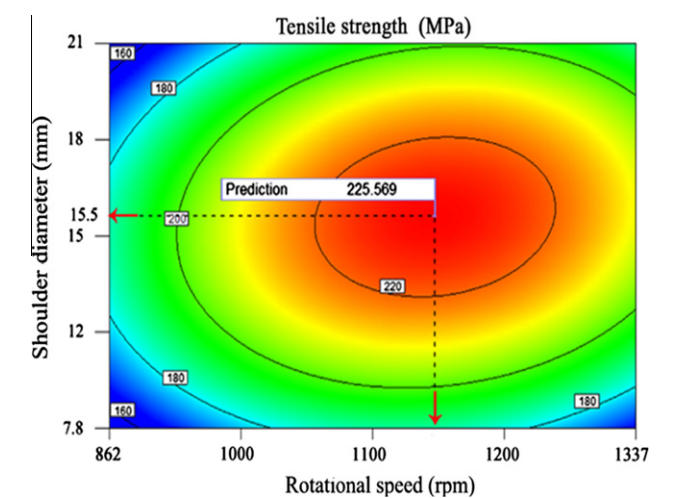


Fig. 6. Contours plot showing the effect of *N* and *D* on the tensile strength at *S* = 80 mm/min, *F* = 7 kN, *D* = 15 mm, *P* = 5 mm, *H* = 45 HRc.

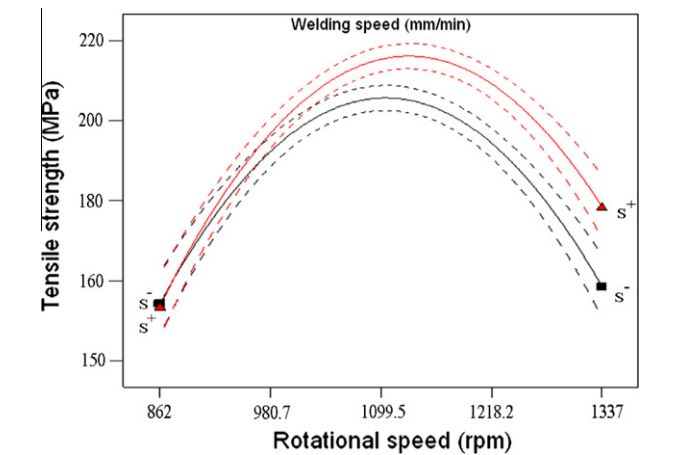


Fig. 7. Interaction effect between *N* and *S* on the tensile strength at *F* = 7 kN, *D* = 15 mm, *P* = 5 mm, *H* = 45HRc.

4.1.1. Effect of process and tool parameters on the responses

In the following sections, whenever an interaction effect or a comparison between any two input parameters is being discussed the other parameters would be on its centre level.

4.1.1.1. Tensile strength. Perturbation plot shown in Fig. 5 illustrates the effect of the friction stir welding parameters on the tensile strength for an optimization design. This graph shows how the response changes as each factor moves from a chosen reference point, with all other factors held constant at the reference value [20]. A steep slope or curvature in a factor indicates that the response is sensitive to that factor. Hence, the plot shows that the

factor rotational speed is mostly influenced the tensile strength followed by factor tool hardness, axial force, shoulder diameter and then welding speed. Fig. 6 is a contour graph shows the effect of the rotational speed and shoulder diameter on the tensile strength. When rotational speed is compared with the shoulder diameter (at a constant tool hardness of 45 HRC, axial force of 7 kN, pin diameter of 5 mm, and welding speed of 80 mm/min) rotational speed is marginally more sensitive to changes in tensile strength as illustrated in Fig. 6.

The interaction effect between the rotational speed and shoulder diameter is more significant than the interaction effect between the other combinations of parameters. In FSW, the tool

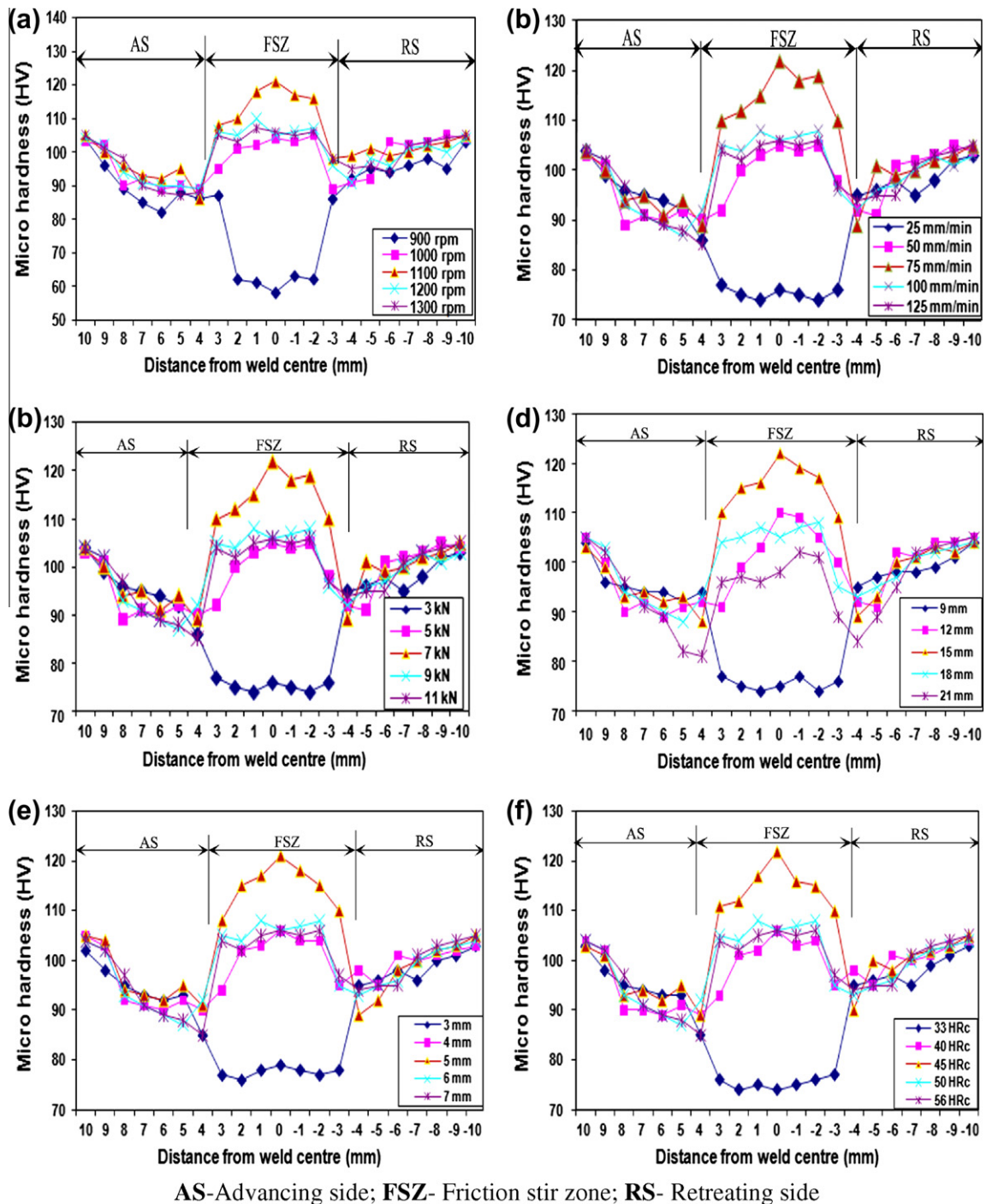


Fig. 8. Effect of process and tool parameters on micro hardness of AA6061-T₆ aluminium alloy. (a) Tool rotational speed. (b) Welding speed. (c) Axial force. (d) Shoulder diameter. (e) Pin diameter. (f) Tool hardness.

rotation speed is more sensitive factor than other parameters. Especially, heat generation due to friction is mainly dependent on tool rotational speed. The friction between the shoulder and work piece results in the biggest component of heating. From the heating aspect, the relative size of pin and shoulder is important. The shoulder also provides confinement for the heated volume of material. The second function of the tool shoulder is to 'stir' and 'move' the material. The uniformity of the microstructure and properties as well as process load is governed by the tool design [21]. Larger shoulder diameter, leads to wider contact area and resulted in wider TMAZ (Thermo-Mechanically Affected Zone) region and HAZ (heat-affected zone) region, subsequently the tensile strength of the joints are deteriorated. As the shoulder diameter increased from 9 mm to 15 mm both the strength and hardness reached a maximum value and then starts to reduce when large shoulder tool was used (21 mm). The smaller shoulder diameter resulted insufficient heat generation due to smaller contact area. The small contact area causes grain growth and severe clustering of precipitates in the stir zone, which resultantly produced lower hardness in the stir zone. The lower tool rotational speed produces less heat generation [22], subsequently heat supplied to the base material is less, which causes insufficient material flow and less plasticization in stir zone and hence, the tensile strength is lower.

The higher tool rotational speed produces high heat generation, subsequently heat supplied to the base material is high, which causes turbulent material flow and grain coarsening in stir zone and hence the tensile strength is lower. Neither low heat input nor high heat input is preferred in FSW, due to the reduction in tensile strength of the joints and it is evident from Fig. 7.

4.1.1.2. Microhardness. Microhardness was measured at mid-thickness region across the weld and the values are presented in Fig. 8. The base metal recorded hardness of 105 HV, which is lower than stir zone but, higher than TMAZ region. The hardness of the stir zone is considerably higher than that of the base metal irrespective of the tool rotational speed used. There are two main reasons for improved hardness in the stir zone. (i) The grain size of stir zone is much finer than that of base metal. The grain refinement plays an important role in material strengthening. According to the Hall–Petch equation, hardness increases as the grain size decreases. (ii) The small intermetallic particles improve the hardness, according to the Orowan hardening mechanism [23]. The difference in hardness between the heat-affected zone and stir zone is attributed to the grain refinement in the stir zone. Fig. 8a shows the lowest hardness was recorded in the joint fabricated with a tool rotational speed of 900 rpm at the TMAZ region of retreating side. Retreating side (RS) recorded appreciably lower hardness values compared to advancing side (AS) irrespective of the welding parameters. The joint fabricated with a tool rotational speed of 1100 rpm recorded the highest hardness value of 121 HV in the stir zone region. Similarly, the welding speed of 80 mm/min (Fig. 8b), axial force of 8 kN (Fig. 8c), shoulder diameter of 15 mm (Fig. 8d), pin diameter of 5 mm (Fig. 8e), tool hardness of 45 HRC (Fig. 8f), resulted in maximum hardness compared to process parameters, and this may be one of the reasons for superior strength of the joints fabricated at above conditions.

4.1.1.3. Corrosion rate. Although aluminium forms a protective aluminium oxide layer on the surface, this thin layer can be breached in aggressive environments leading to corrosion. In particular, NaCl containing environments lead to the formation of aluminium chlorides which in turn reduce the effectiveness of the oxide layer in preventing corrosion. For that reason, the effect of friction stir-welding input parameters on corrosion behavior of the welds was investigated. The result demonstrates that all the input parameters have a significant effect on the corrosion rate of the

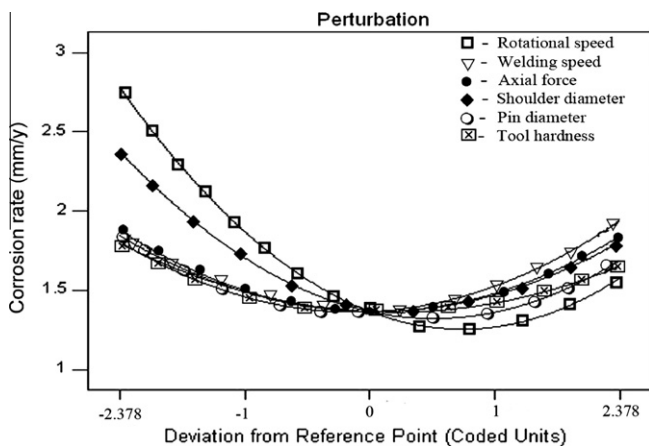


Fig. 9. Perturbation plot showing the effect of all factors on the corrosion rate.

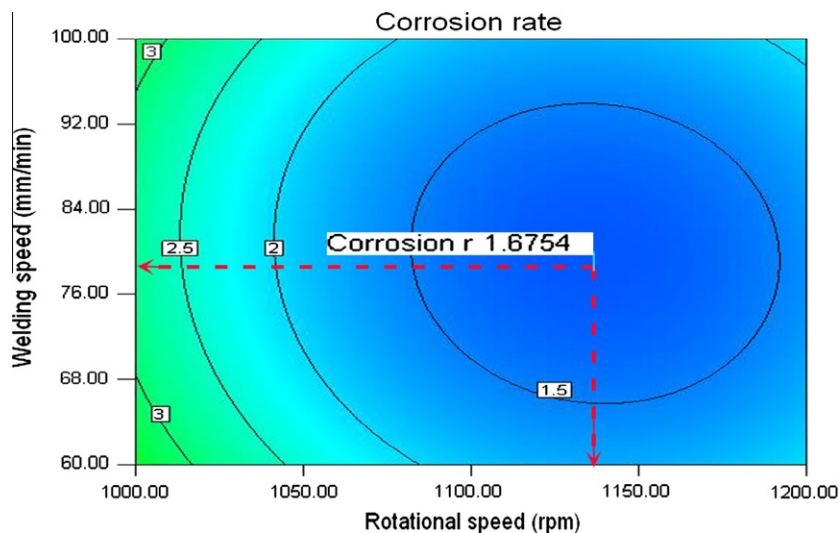


Fig. 10. Contours plot showing the effect of N and P on the corrosion rate at $S = 80$ mm/min, $F = 7$ kN, $D = 15$ mm, $H = 45$ HRC.

welded joint. Fig. 9 shows a perturbation plot to compare the effect of different factors at a particular point (mid-point by default) in the design space. From this Fig. 9, it can be noticed that the corrosion rate is minimum as the rotational speed in centre level, whereas at lower or higher tool rotational speeds, the corrosion rate is maximum. Similarly, the joint fabricated at the welding speed of 80 mm/min, force of 7 kN, with a shoulder diameter of 15 mm, pin diameter of 5 mm and hardness of 45 HRC yielded the lower corrosion rate. The results demonstrated that the lowest corrosion rate could be obtained when all the FSW input parameters were at their middle level. Fig. 10 shows the effect of the rotational speed and shoulder diameter on the corrosion rate at a welding speed of 80 mm/min, axial force 7 kN, pin diameter 5 mm and tool hardness 45 HRC. The results indicate that as the tensile strength increases, the corrosion rate decreases.

4.1.1.4. Optimization. The issue of linking the tensile strength and corrosion resistance must be addressed as any increase in the strength is usually reflected in deteriorating the corrosion resistance. As a consequence, both strength and corrosion resistance are usually studied together. On balance, and based on the above discussion, it is better to run an optimization study to find out the optimal welding conditions at which the desirable mechanical properties of the welded joint can be achieved. In fact, once the models have been developed and checked for adequacy, the optimization criteria can be set to find out the optimum welding conditions. In this investigation, two criteria were implemented to maximize both the tensile strength and hardness. The first criteria were to reach the maximum tensile strength and hardness with no

limitation on either the welding parameters or the corrosion rate. While, in the second criteria the goal was to reach the maximum tensile strength and hardness at relatively low-corrosion rate by using maximum rotational speed and welding speed. Table 6 summarizes these two criteria. While Tables 7 and 8 present the optimal solution based on the two optimization criteria is determined by design-expert software. The optimization results clearly demonstrated that whatever (the optimization criteria), the rotational speed has to be around its centre limit of 1100 rpm to achieve the maximum tensile and hardness. This result support the discussion made earlier on the effect of rotational speed on the responses. Table 7 presents the optimal welding conditions according to the first criteria that would lead to the maximum tensile and hardness of about 225 MPa and 124 HV respectively, at high corrosion rate of about 1.30×10^{-4} mm/y. But, if the corrosion rate is to be reduced much further with approximate percentage of 22% with acceptable tensile and hardness, the rotational speed has to be maximized to its highest value and a welding speed of 84.6 mm/min has to be used instead of 92.04 mm/min. In this case, the tensile strength and hardness would be about 224 MPa and 122 HV at corrosion rate of about 1.67×10^{-4} mm/y respectively, as can be seen in Table 8. It is obvious that the graphical optimization allows visual selection of the optimum welding conditions according to certain criteria. The result of the graphical optimization are the overlay plots, this type of plots are extremely practical for quick technical use in the workshop to choose the values of the welding parameters that would achieve certain response value for this type of material. The yellow/shaded areas on the overlay plots Figs. 11 and 12 are the regions that meet the proposed criteria.

Table 6
Optimization criteria used in this study.

Parameter and responses	Limits		Importance	First criterion	Second criterion
	Lower	Upper			
Rotational speed (rpm)	1000	1200	3	In range	Maximize
Welding speed (mm/min)	60	100	3	In range	Maximize
Axial force (kN)	6	8	3	In range	In range
Shoulder diameter (mm)	12	18	3	In range	In range
Pin diameter (mm)	4	6	3	In range	In range
Tool hardness (HRC)	40	50	3	In range	In range
Tensile strength (MPa)	165	226	5	Maximize	Maximize
Hardness (HV)	58	123	5	Maximize	Maximize
Corrosion rate (mm/y)	1.53×10^{-4}	8.15×10^{-4}	3	In range	Minimize

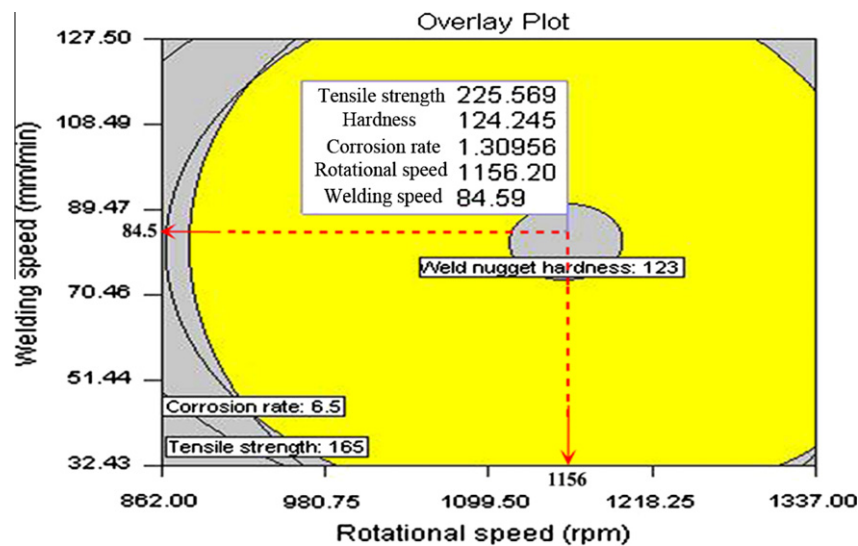
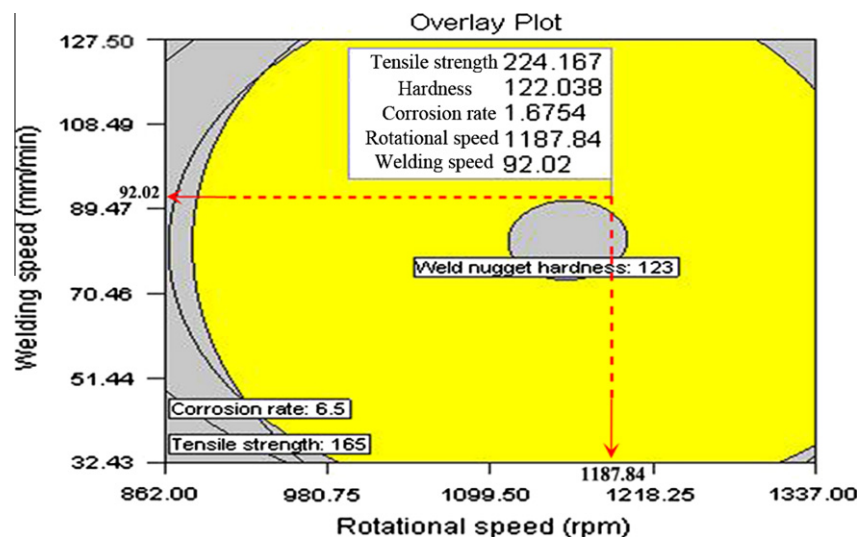
Table 7
Optimal solution as obtained by design-expert based on the first criterion.

Experimental details							Results			
Exp. No.	Input parameters						Responses			
	N	S	F	D	P	H	TS (MPa)	H (HV)	CR (mm/y) $\times 10^{-4}$	Desirability
1	1156.11	84.57	7.17	15.71	5.21	44.85	225.569	124.251	1.30859	0.996457
2	1155.97	84.63	7.18	15.71	5.21	44.84	225.568	124.241	1.31024	0.996457
3	1156.13	84.59	7.17	15.71	5.21	44.84	225.568	124.251	1.30836	0.996457
4	1156.29	84.57	7.18	15.70	5.20	44.84	225.568	124.242	1.31054	0.996457
5	1156.06	84.58	7.17	15.70	5.21	44.85	225.568	124.254	1.30886	0.996456
6	1155.75	84.61	7.17	15.71	5.21	44.85	225.568	124.252	1.30794	0.996456
7	1156.23	84.60	7.17	15.69	5.20	44.84	225.568	124.24	1.3105	0.996456
8	1155.95	84.51	7.17	15.70	5.21	44.84	225.568	124.253	1.30787	0.996456
9	1156.62	84.57	7.17	15.71	5.21	44.83	225.568	124.245	1.30978	0.996456
10	1156.18	84.66	7.18	15.69	5.21	44.83	225.568	124.242	1.31172	0.996455
11	1155.97	84.59	7.17	15.69	5.20	44.86	225.568	124.252	1.30916	0.996455
12	1155.91	84.67	7.17	15.71	5.21	44.87	225.568	124.251	1.30945	0.996455
13	1155.90	84.65	7.18	15.69	5.20	44.84	225.568	124.229	1.31112	0.996455
14	1156.63	84.58	7.18	15.70	5.20	44.84	225.568	124.242	1.31314	0.996454
15	1156.08	84.55	7.17	15.71	5.21	44.87	225.568	124.272	1.30803	0.996453

Table 8

Optimal solution as obtained by design-expert based on the second criterion.

Experimental details							Results			
Exp. No.	Input parameters						Responses			
	N	S	F	D	P	H	TS (MPa)	H (HV)	CR (mm/y) $\times 10^{-4}$	Desirability
1	1187.66	92.04	7.07	15.75	5.27	45.21	224.172	122.037	1.67437	0.808734
2	1187.87	92.04	7.07	15.75	5.27	45.22	224.161	122.031	1.67609	0.808734
3	1187.94	92.03	7.07	15.75	5.26	45.23	224.16	122.023	1.67582	0.808734
4	1187.85	92.00	7.08	15.76	5.27	45.22	224.178	122.055	1.67559	0.808733
5	1187.63	92.00	7.07	15.74	5.27	45.22	224.177	122.057	1.6727	0.808733
6	1188.13	92.06	7.08	15.75	5.27	45.23	224.153	122.019	1.68003	0.808733
7	1187.86	92.02	7.08	15.74	5.27	45.20	224.171	122.034	1.67566	0.808733
8	1187.56	92.09	7.07	15.76	5.27	45.23	224.161	122.024	1.67524	0.808733
9	1187.42	92.00	7.07	15.77	5.27	45.21	224.185	122.062	1.67121	0.808731
10	1187.52	91.23	7.05	15.22	5.26	45.21	224.10	122.01	1.67254	0.80782
11	1186.32	91.32	7.06	15.21	5.21	45.23	224.06	121.36	1.662	0.80784
12	1185.45	92.32	7.08	15.25	5.32	45.65	223.06	121.65	1.664	0.80684
13	1188.13	92.06	7.08	15.75	5.27	45.23	224.153	122.019	1.68003	0.808733
14	1187.86	92.02	7.08	15.74	5.27	45.20	224.171	122.034	1.67566	0.808733
15	1187.56	92.09	7.07	15.76	5.27	45.23	224.161	122.024	1.67524	0.808733

**Fig. 11.** Overlay plot shows the region of optimal welding condition based on the first criterion at $F = 7$ kN, $D = 15$ mm, $P = 5$ mm, $H = 45$ HRC.**Fig. 12.** Overlay plot shows the region of optimal welding condition based on the second criterion at $F = 7$ kN, $D = 15$ mm, $P = 5$ mm, $H = 45$ HRC.

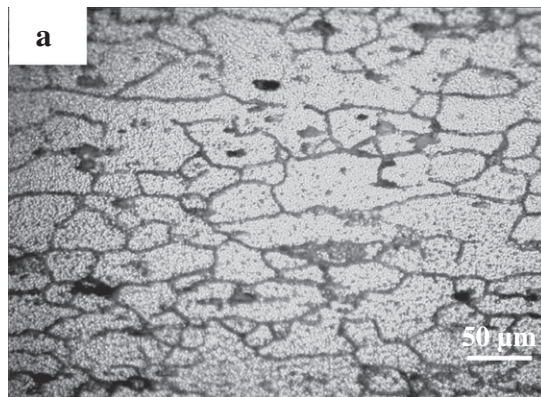
4.2. Validation of the developed models

To validate the developed models, three confirmation experiments were carried out with the welding conditions chosen randomly from the optimization results. For the actual responses the average of three measured results was calculated. Table 9 summarizes the experimental condition, the average of actual experimental values, the predicted values and the percentages of error. The optimum values of process parameters and average tensile strength of friction stir welded AA6061-T₆ aluminium alloy was

found to be 226 MPa, which shows the excellent agreement with the predicted values. The base metal micrograph of Fig. 13a contains a coarse and elongated grain. But in the traverse section of FSW joint fabricated using optimum parameters reveals that there is no defect due to sufficient heat generation and contains finer grains that appear weld zone as shown in Fig. 13b. The average grain diameter was measured in stir zone and it was found to be finer (9 μm), compared to base metal (50 μm). The fractured surfaces of the tensile tested specimens were characterized using SEM (scanning electron microscope) to understand the failure pat-

Table 9
Validation test results.

Experimental details							Results			
Exp. No.	Input parameters						Responses			
	<i>N</i>	<i>S</i>	<i>F</i>	<i>D</i>	<i>P</i>	<i>H</i>		TS (MPa)	H (HV)	CR (mm/y)
1	1156.11	84.57	7.17	15.71	5.21	44.85	Actual	220	120	1.301×10^{-4}
							Predicted	225.569	124.251	1.308×10^{-4}
							Error%	2.46	3.42	0.53
2	1156.62	84.57	7.17	15.71	5.21	44.83	Actual	221	121	1.303×10^{-4}
							Predicted	225.568	124.245	1.309×10^{-4}
							Error%	2.02	2.61	0.45
3	1155.91	84.67	7.17	15.71	5.21	44.87	Actual	221	122	1.302×10^{-4}
							Predicted	225.568	124.251	1.309×10^{-4}
							Error%	2.02	1.81	0.534

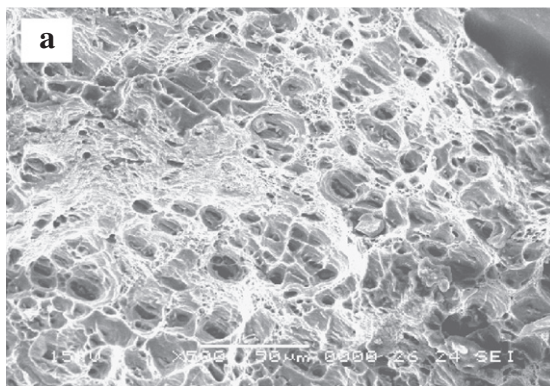


(a) Base metal

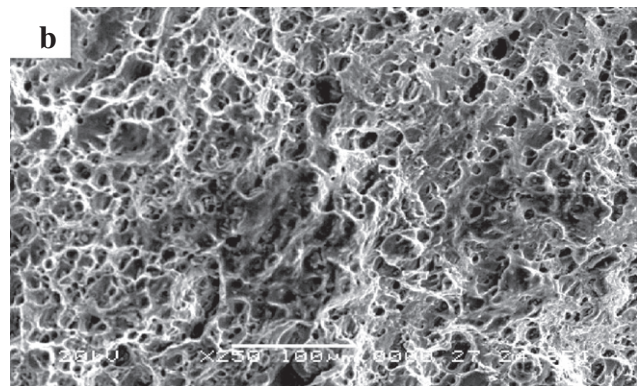


(b) Stir zone (optimum condition)

Fig. 13. Optical micrographs.



(a) Base metal



(b) Stir zone (optimum condition)

Fig. 14. SEM fractographs of tensile specimens.

terns. All the fractured surfaces invariably consist of dimples, which is an indication that the mode of failure is ductile. The fractured surface of the base metal Fig. 14a shows coarse dimples than the stir zone Fig. 14b.

5. Conclusions

Using the friction stir welding machine, within the limits of the process parameters and tool parameters considered in this study, the following points can be concluded:

1. Multi objective optimization using RSM is an useful technique to optimize the friction stir welding parameters to obtain the maximum tensile strength without deteriorating the corrosion resistance of FSW joints.
2. A tool rotational speed between 1155 and 1157 rpm is an optimum input to obtain an excellent welded component produced from AA6061-T₆ aluminium alloy. The welding speed is the most predominant welding parameter and its interaction with the rotational speed should be monitored. Welding speed between 84.51 and 84.67 mm/min is compatible with axial force 7.17 kN, while shoulder diameter 15.71 mm, pin diameter of 5.21 mm and tool hardness 44.85 HRC is compatible.
3. The joint fabricated with a tool rotational speed of 1100 rpm recorded the highest tensile strength and hardness value of 121 HV in the stir zone region. Similarly the welding speed of 80 mm/min, axial force of 8 kN, shoulder diameter of 15 mm, pin diameter of 5 mm and tool hardness of 45 HRC, resulted in maximum strength properties compared to other process parameters. The corrosion rate can be reduced by minimum with acceptable mechanical properties if the optimal welding conditions are used.

Acknowledgements

The authors are grateful to the Department of Manufacturing Engineering, Annamalai University, Annamalai Nagar, India for extending the facilities of Material Testing Laboratory to carry out this investigation. The authors wish to place their sincere thanks to Clean Technology Division of Ministry of Environment and Forest, Government of India, New Delhi for financial support rendered through a R&D Project No. MoEF1-9/2005-CT.

References

- [1] Thomas WM. Friction stir welding. International patent application No. PCT/GB92/02203 and GB patent application No. 9125978.8. US Patent No. 5, 460, 317; 1991.
- [2] Dawes CJ. An introduction to friction stir welding and its development. *Weld Metal Fabric* 1995;63:2–16.
- [3] Thomas WM, Nicholas ED. Friction stir welding for the transportation industries. *Mater Des* 1997;18:269–73.
- [4] Oosterkamp A, Djapic Oosterkamp L, Nordeide A. Kissing bond phenomena in solid state welds of aluminum alloys. *Weld J* 2004;225–31.
- [5] Zeng WM, Wu HL, Zhang J. Effect of tool wear on microstructure mechanical properties and acoustic emission of friction stir welded 6061 Al alloys. *Acta Metall Sin* 2006;19(1):9–19.
- [6] Valerio Flores Olga. Micro structural issues in a friction stir welded aluminium alloy. *Scripta Mater* 1998;38(5):703–8.
- [7] Jayaraman M, Sivasubramanian R, Balasubramanian V, Lakshminarayanan AK. Prediction of tensile strength of friction stir welded A356 cast aluminium alloy using response surface methodology and artificial neural network. *J Manuf Sci Prod Res* 2008;9:1–21.
- [8] Elangovan K, Balasubramanian V. Developing an empirical relationship to predict tensile strength of friction stir welded AA2219 aluminium alloy joints. *J Mater Eng Perform* 2008;17:820–30.
- [9] Lombord H, Hattingh DG, Steuwer A, James MN. Optimising FSW process parameters to minimise defects and maximise fatigue life in 5083-H321 aluminium alloy. *J Eng Fract Mech* 2008;75:341–54.
- [10] Rajakumar S, Muralidharan C, Balasubramanian V. Optimization of the friction-stir-welding process and the tool parameters to attain a maximum tensile strength of AA7075-T₆ aluminium alloy. *J Eng Manuf* 2010;224:1175–91.
- [11] Lakshminarayanan AK, Balasubramanian V. Process parameters optimization for friction stir welding of RDE-40 aluminium alloy using Taguchi technique. *Trans Nonferr Metal Soc China* 2008;18:548–54.
- [12] Montgomery DC. Design and analysis of experiments. 2nd ed. New York: John Wiley and Sons; 1984.
- [13] Rajakumar S, Muralidharan C, Balasubramanian V. Establishing empirical relationships to predict grain size and tensile strength of friction stir welded AA6061-T₆ aluminium alloy joints. *Trans Nonferr Soc China* 2010;20:1863–72.
- [14] William G Cochran, Gertrude M Cox. Experimental designs. 2nd ed. New York: John Wiley and Sons; 1957.
- [15] Johnson N, Leona FC. Statistics and experimental design in engineering and physical sciences, vol. 2. New York: John Wiley and Sons; 1964.
- [16] Myers RH, Montgomery DC. Response surface methodology—process and product optimization using designed experiment. London: John Wiley; 1995.
- [17] Design-Expert software v8 user's guide. Technical manual. Minneapolis (MN): Stat-Ease Inc.; 2010.
- [18] ASTM E8 M-04. Standard test method for tension testing of metallic materials. ASTM International; 2006.
- [19] ASTM G31-72. Standard practice for laboratory immersion corrosion testing of metals; 2002.
- [20] Sivakumar T, Manavalan R, Muralidharan C. An Improvement HPLC method with the aid of a chemometric protocol: simultaneous analysis of amlodipine and atorvastatin in pharmaceutical formulations. *J Sep Sci* 2007;30:3143–52.
- [21] Rajakumar S, Muralidharan C, Balasubramanian V. Influence of friction-stir-welding process and tool parameters on strength properties of AA7075-T₆ aluminium alloy joints. *Mater Des* 2011;535–49.
- [22] Balasubramanian V. Relationship between base metal properties and friction stir welding process parameters. *Mater Sci Eng A* 2009;480:397–403.
- [23] Wang XH, Wang KS. Microstructure and properties of friction stir butt-welded AZ31 magnesium alloy. *Mater Sci Eng A* 2006;431:114–7.